during a filament activation? What are the causes of filament eruption? What is the nature of the coronal environment around the eruptive filament? Is there a difference between filaments — those activated in the presence of new magnetic flux and those which are not? Are there two distinct classes of precursor — with and without active filaments?

Velocity and Magnetic Shear How are they related to each other and to flare productivity? What is the role of the resulting electric currents? Is there a critical value of shear for eruptive instability? What are the preflare characteristics of the velocity field and how do they evolve?

Emerging Flux What are the necessary and sufficient conditions for it to trigger a large flare? What is different in the numerous flux emergences which produce no large flares? What are typical velocities, magnetic field strengths and rates of growth? Are they related to particle acceleration?

1.2 MAGNETOHYDRODYNAMIC INSTABILITY

E.R. Priest, P. Cargill, T.G. Forbes, A.W. Hood and R.S. Steinolfson

1.2.1 Magnetic Reconnection

Our basic understanding of magnetic reconnection has changed recently due to the beginning of detailed numerical experiments on various aspects of the process (Priest 1984a and 1984b). These have linked the two previous strands of reconnection theory, namely tearing mode instability and Petschek-Sonnerup reconnection (as described below), and have presented us with new surprises (§1.2.2, 1.2.3).

1.2.1.1 Linear Tearing Modes

A current sheet of width d is spontaneously unstable to the linear tearing mode (Furth *et al.*, 1963), which creates long thin magnetic islands by reconnection on a time-scale

(1.2.1)

where $\tau_d = d^2\eta$ is the resistive diffusion time and $\tau_A = d/v_A$ is the Alfven time in terms of the Alfven speed (v_A). For the active-region corona with global length-scales (d) of typically 10^3-10^4 km, the tearing mode growth-time (1.2.1) is days to weeks and is therefore much too long to explain a flare although it may well be important for normal coronal heating, (Heyvaerts and Priest 1985; Parker 1984).

Tearing may also take place in a sheared magnetic field such as a flux tube. However, in solar coronal applications it is important to incorporate the stabilising effect of photospheric line tying, since the footpoints of coronal magnetic field lines are anchored in the dense photosphere. This has led to suggestions that the resistive modes be completely stable in a loop (Mok and Van Hoven 1982) or in an arcade (Hood 1984a, Migliuolo and Cargill 1983) unless there is a reversal in the axial (loop) or azimuthal (arcade) field component.

An important new development is the discovery of a much faster radiative tearing mode (Van Hoven *et al.*, 1982, Steinolfson 1983, 1984a, 1984b). Steinolfson and Van Hoven have solved the normal incompressible resistive MHD equations but they have allowed the magnetic diffusivity to depend on temperature ($\eta = \eta_0 T^{-3/2}$), which introduces a coupling to the energy equation

$$\frac{nk_B}{\gamma-1}\frac{dT}{dt} = \nabla\cdot(\kappa B\, B\cdot\nabla T) - R_p T^{-\alpha} + \mu_0\eta(T)J^2, \quad (1.2.2)$$

and produces resistive field changes on energy-transport time scales.

The predicted growth rate of linearly unstable modes is shown in Figure 1.2.1. At coronal values of the magnetic Reynolds number S (typically $S_s = 10^{10.6}$ for $T = 10^6$ K, $n = 10^{17}$ m^{-3}, B = 100 G, a = 100 km) there are two distinct modes, namely the tearing mode and the radiative mode, which is typically a hundred times faster. However, both modes are modified significantly. Local cooling at the X-points increases the magnetic diffusivity and so enhances the reconnection for the tearing mode. In the radiative mode a considerable amount of reconnection is present (Figure 1.2.2): the island width is typically 30% of that produced by the tearing mode and the perturbed magnetic energy is typically five times the perturbed thermal energy.

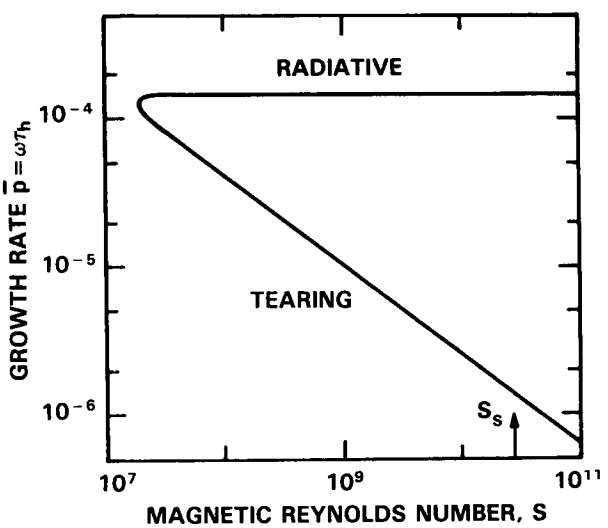

Figure 1.2.1 Growth rate(ω) for radiative tearing instability in units of the Alfven travel time ($\tau_A = a/v_A$) as a function of the magnetic Reynolds number ($S = \tau_d/\tau_h$), where $\tau_d = a^2/\eta$ is the diffusion time. Here the dimensionless wavenumber (ka) is 0.1, corresponding to a wavelength of 10π times the shear length (a), (From Steinolfson and Van Hoven 1984).

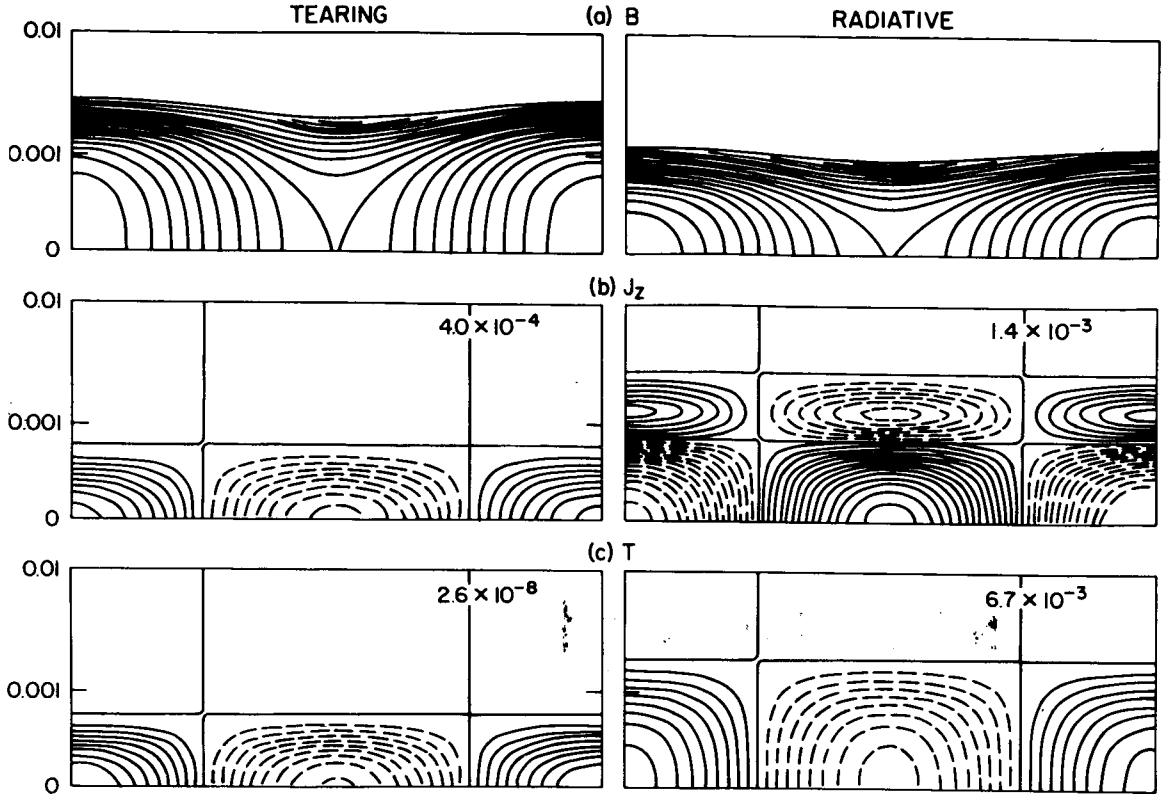

Figure 1.2.2 A comparison of the magnetic field (B), electric current (J_z), temperature (T) and ohmic dissipation ($\mu_o \eta j^2$) for the tearing and radiative modes at $S = S_s$. Contours are normalised with respect to the maximum values indicated in the top right of each box, and the y scale is expanded. Dashed (and solid) contours represent values that are below (and above) the initial values. (From Steinolfson and Van Hoven, 1984).

The inclusion of compressibility is found to be unimportant for solar coronal conditions. It inverts the tearing temperature at very long wavelengths and increases the radiative rate by typically a factor of five at very short wavelengths. Steinolfson (1984) includes perpendicular thermal conduction which introduces spatial temperature oscillations normal to the tearing surface and on a scale comparable with the width of the resistive tearing layer. Such thermal ripples create velocity oscillations but don't affect the magnetic field. Steinolfson (1983) derives analytical expressions for the growth-rates in the constant-ψ and long-wavelength approximations. He finds that for S smaller than about 10^6 the modes are generally stabilised. Also, he discusses the Joule heating instability which is present in the absence of radiation.

1.2.1.2 Petschek-Sonnerup Reconnection

The second main theme of reconnection theory has been the fast nonlinear mode of steady Petschek-Sonnerup reconnection (Petschek 1964, Sonnerup 1970), which has been reviewed many times (e.g., Priest 1984b, Vasyliunas 1975). In this fast nonlinear state the current sheet bifurcates into two pairs of slow shock waves, which exist because the inflow plasma speed exceeds the slow magnetoacoustic wave speed. The shocks are standing in the flow and, as the plasma and magnetic field lines pass through them, they have the effect of transferring inflowing magnetic energy into the heat and kinetic energy of hot fast jets.

In general one would expect the external boundary conditions at the sources of the inflowing plasma to produce a hybrid Petschek-Sonnerup regime. Particular forms of those boundary conditions (namely free or fixed corner conditions) may, however, produce the pure Petschek or Sonnerup extremes, respectively (Vasyliunas 1975). The difference between the two extremes is as follows. The Petschek mode has a pure fast magnetoacoustic expansion in the inflow regions upstream of the slow shocks, such that the flow converges and the magnetic field strength decreases as the central diffusion region is approached. By contrast, the inflow region for the Sonnerup mode consists of a slow mode expansion with the flow diverging and the field strength increasing. Although in Sonnerup's original analysis the slow mode expansion fan was very thin and generated at a single point in the inflow, Sonnerup reconnection here refers also to the more general situation with a wide fan and generation across a substantial part of the inflow region.

When the reconnection develops locally from the tearing of a sheared magnetic field, such as in the simulation of the Kopp-Pneuman model for main phase reconnection (§1.2.5), the nonlinear steady state is expected to be Petschek-like (Figure 1.2.9). When the reconnection is driven from outside, as in a simulation of emerging flux (§1.2.4), the nonlinear state can be closer to the Sonnerup regime (Figure 1.2.7).

Recent numerical experiments by Forbes and Biskamp have produced two main surprises. They have demonstrated that the tearing mode can develop in its nonlinear phase into the fast Petschek-Sonnerup mode (§1.2.2). They have also revealed some new regimes of fast nonlinear unsteady reconnection when the Petschek-Sonnerup mode breaks down or goes unstable (§1.2.3).

1.2.2 Nonlinear Tearing

The nonlinear development of the tearing mode is far from simple and not yet completely understood. Several pathways along which the instability may develop appear to be possible, depending on the geometry and the parameter regime, as outlined below.

1.2.2.1 Saturation

The first possibility is that the mode may saturate at an extremely low amplitude, when the island width has only grown equal to the resistive layer width (Rutherford 1973). This benign outcome with an extremely small energy release has been the most commonly expected development in laboratory devices. However, some recent calculations have been performed by Steinolfson and Van Hoven at large values of S ($\simeq 10^6$) and at long wavelengths, conditions much more appropriate to solar applications than previous attempts (Steinolfson and Van Hoven 1983). At a wavelength of only twice the shear length (a) the reconnection is indeed found to slow down drastically, as in the Rutherford regime. But at wavelengths of 20a the nonlinear reconnection rate is ten times faster and the island grows enormously up to a width of 2a (see also §1.2.3.2).

1.2.2.2 Mode Coupling

In a magnetic flux tube, surfaces at different radii are unstable to modes with different values of m. m = 1 represents a simple kinking of the tube near the surface, with the cross-section remaining circular. For higher m values the cross-section becomes distorted: for instance, m = 2 perturbs the tube to a double-helix shape and m = 3 to a triple helix. Normally, one expects several such modes to be present and, when they grow to a large enough amplitude, modes on neighbouring surfaces may couple to one another (Waddell *et al.*, 1978).

Aydemir and Barnes (1984) have performed some numerical studies for a reversed field pinch which may be of relevance to coronal structures. Such a toroidal laboratory device possesses a toroidal field component (B_s) and a toroidal current (I_s) which produces a poloidal field component (B_θ) of the same order of magnitude.

Experimentally, an initially turbulent state leads to a spontaneous reversal of the field near the axis followed by a long quiescent phase. In this state the magnetic field is near to a constant-α force-free field which, according to Taylor's hypothesis (1974), minimises the magnetic energy subject to toroidal-flux and magnetic-helicity conservation. Heyvaerts and Priest (1984) have generalised the hypothesis and applied it to the corona in order to deduce the coronal heating and mini-flarings that are produced by tearing turbulence.

Aydemir has studied the relaxation and sustenance of the quiescent state using an incompressible 3D MHD code, with $S \simeq 5 \times 10^3$. The torus is approximated by a periodic cylinder of length $2\pi R_0$, and so the variables are Fourier expanded in the axial and azimuthal directions.

Starting from an unstable equilibrium the nonlinear evolution is followed, with the dominant modes having m = 1 and n = 2 and 3. The system is driven in the sense that the toroidal current is maintained against resistive diffusion by an external source. For a 2D single helicity calculation, in which only those modes with a given ratio m/n are retained, a steady helical magnetic field is maintained in a laminar manner. For a 3D multiple helicity calculation, when two modes such as m/n = 1/2 and 1/3 are perturbed, many other modes are generated by nonlinear coupling. Below a critical current (such that $\alpha a \simeq 3$) the field evolves to a steady state, and above that value a quasi-steady state is reached with fluctuations about a mean value maintained by a turbulent dynamo for at least 1000 τ_A. Also, for some currents a bifurcation or frequency doubling is observed. Another important effect is that the magnetic flux surfaces break up and the field lines become stochastic, which produces a rapid increase in heat transport across the magnetic field.

1.2.2.3 Coalescence

In the linear regime the fastest growing tearing mode has a very long wavelength ($\simeq S^{1/4}a$), and so in many cases only one magnetic island will form. Sometimes, however, the structure may be long enough for several islands to grow, and then, in the nonlinear regime, neighbouring islands may be attracted towards one another by an ideal mode known as the coalescence instability (Finn and Kaw, 1977, Pritchett and Wu, 1979). Being an ideal instability, unlike the tearing mode, this mode grows extremely rapidly on Alfvenic times.

The results of numerical simulation by Bhattacharjee, Brunel and Tajima (1983) are shown in Figure 1.2.3b for a plasma β of 0.02 and a magnetic Reynolds number of 10^3. They begin with two magnetic islands in equilibrium, which are assumed to have been created by tearing (first frame).

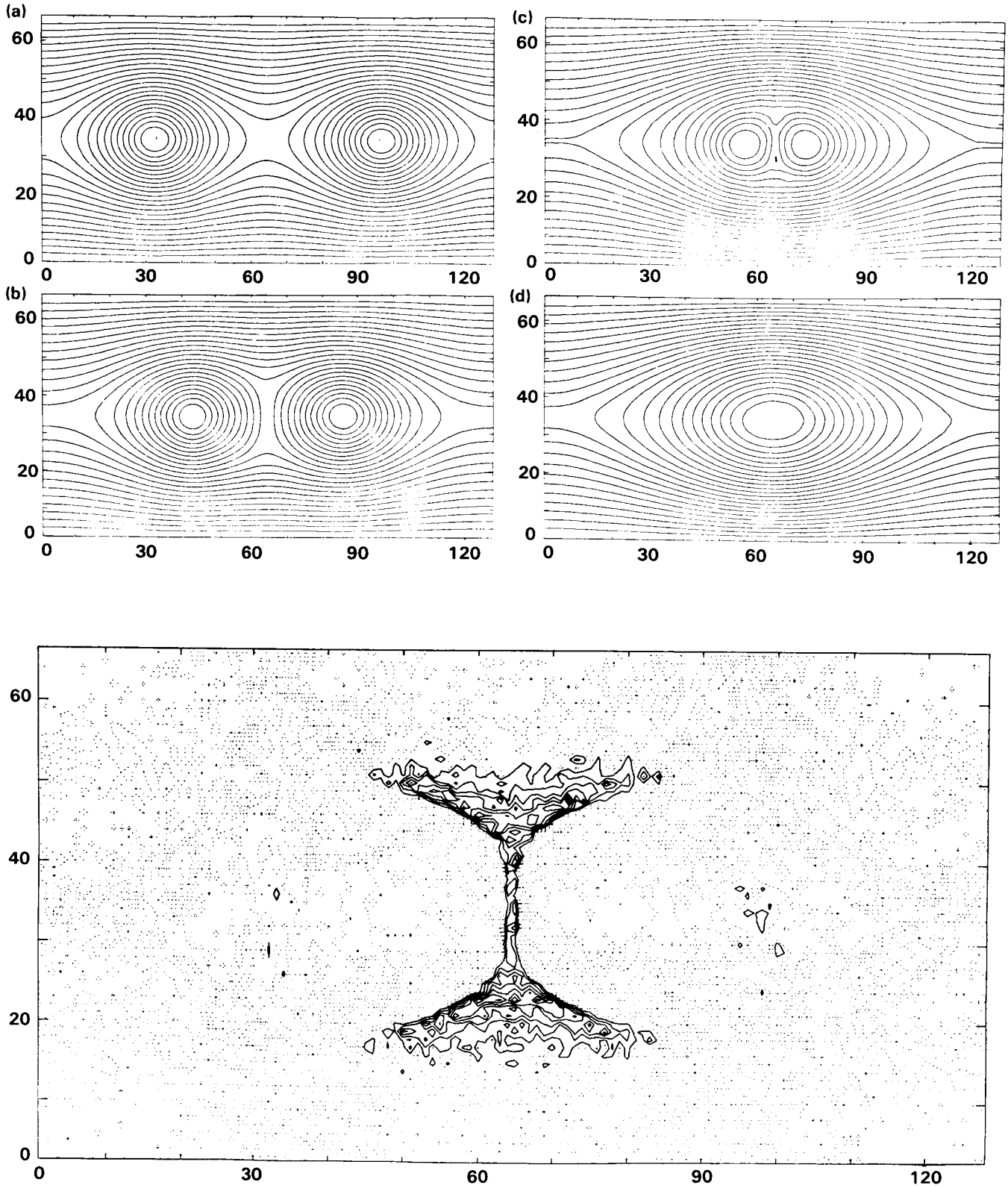

Figure 1.2.3 A numerical simulation of the coalescence instability showing (a) magnetic field lines at several times (b) plasma density contours. (From Bhattacharjee *et al.,* 1983).

The two islands rapidly approach one another and create an intense current sheet at the interface between them as the coalescence instability saturates (second frame). Then the two islands reconnect (third frame) and coalesce to form a single island (fourth frame), which oscillates in response to its violent birth. Plasma density contours at the beginning of the reconnecting phase (Figure 1.2.3b) at $t = 1.6L/v_A$, where $L = 128$ is the length of the system, suggest the presence of two pairs of slow shocks propagating from the ends of the central current sheet. Also, the large length of the central current sheet and the high speed of approach of the two islands suggest that this may represent a flux pile-up regime (§1.2.3.1).

1.2.2.4 Petschek-Sonnerup Reconnection

When the outflow boundary conditions are free enough and the inhibiting effect of the large tokamak axial field is absent, it is possible for the tearing mode to evolve nonlinearly into the fast steady state of Petschek-Sonnerup reconnection (Forbes and Priest, 1982, 1983a), as described in Section 1.2.1.2. A new discovery by Forbes is that fast-mode shocks may be present in the outflowing hot jets (Forbes and Priest, 1983a, 1983b). These have the effect of degrading the kinetic energy into heat and may be much more efficient at accelerating fast particles than the much thicker slow shocks. The steady Petschek-Sonnerup mode is possible when the inflow speed (v) of plasma at large distances is less than a maximum value, $v < v_{max}$, which depends on the magnetic Reynolds number and also on the external boundary conditions. For pure Petschek reconnection it is typically 0.01 v_A, but for pure Sonnerup reconnection it is roughly the Alfven speed (v_A).

1.2.3 Nonlinear Reconnection Experiments

1.2.3.1 New Regimes of Fast Reconnection

Recent numerical experiments at high magnetic Reynolds number by Forbes (Forbes and Priest, 1982, 1983a, 1983b) and by Biskamp (1982a, 1982b, 1982c) have revealed two new regimes of fast unsteady reconnection when the Petschek-Sonnerup mode breaks down (Figure 1.2.4).

The *flux pile-up regime* occurs when the inflow of plasma is so fast that ($v > v_{max}$) is violated, as for instance when reconnection is driven by an ideal instability such as coalescence or kinking. In this case the flux cannot reconnect as fast as it is brought in and so it piles up outside the central diffusion region and causes it to grow in length.

The *impulsive bursty regime* occurs when the length (L) of the central diffusion region in either the Petschek-Sonnerup or flux pile-up regime becomes too great

(1.2.3)

In this case the central sheet goes unstable to secondary tearing (on the tearing mode time-scale) and coalescence (on the

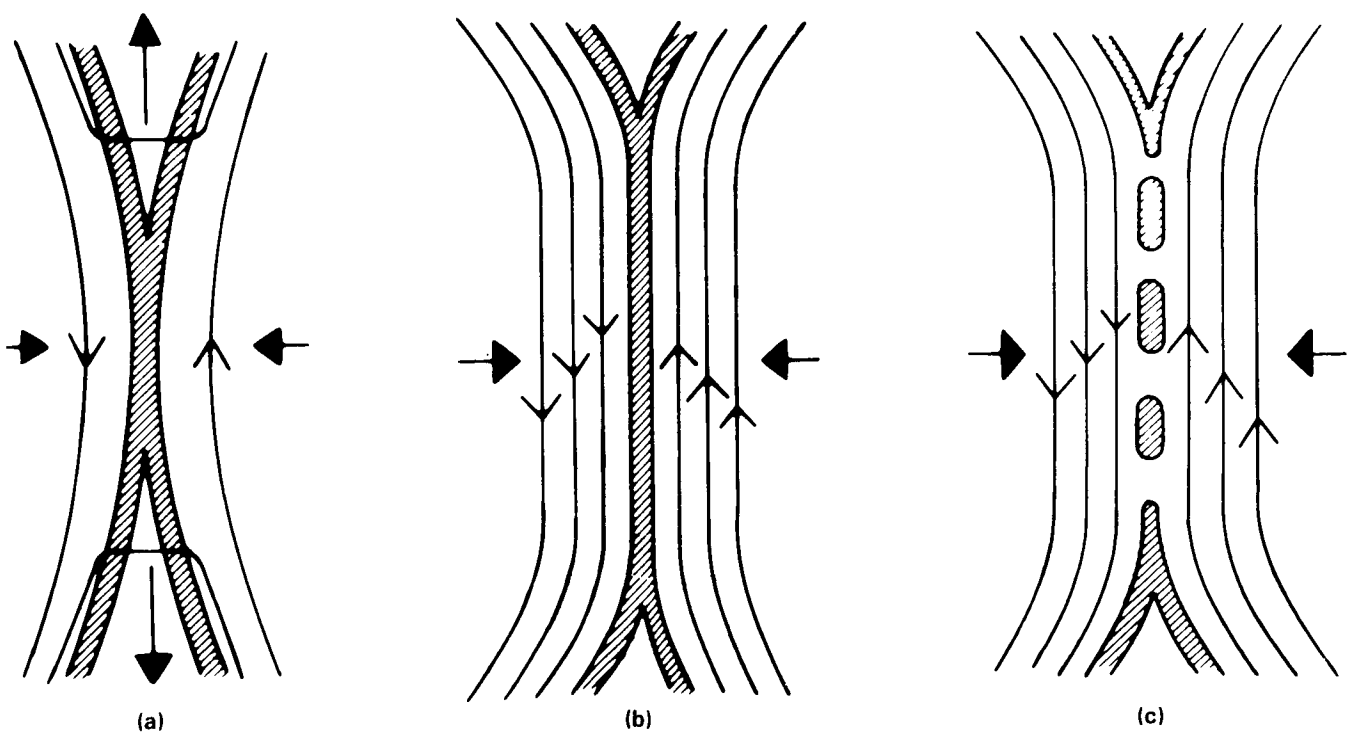

Figure 1.2.4 Regimes of Fast Reconnection: (a) Petschek-Sonnerup, (b) Flux Pile-up, (c) Impulsive Burst. (From Priest, 1984).

Alfven time-scale). The result is a more rapid energy release in a series of bursts as the islands coalesce. This could be extremely important for particle acceleration and the impulsive energy release that is often seen in flares.

1.2.3.2 Nonlinear Tearing at High S

Steinolfson and Van Hoven (1984b) have investigated numerically the nonlinear evolution of the tearing mode at values of Lundquist number (S), (normally equal to the magnetic Reynolds number) between 10^2 and 10^6 and dimensionless wavenumber (α = ka) between 0.042 and 0.5. They find that the growth slows considerably from the linear rate, and at least 80% of the stored magnetic energy is converted into thermal energy for the long wavelength modes with ka < 0.5. Also the maximum electric fields are about three orders of magnitude smaller than the Dreicer field. However, other features depend on the k-S parameter regime, as follows.

The incompressible resistive MHD equations are solved with temperature (T) and magnetic diffusivity (η) assumed constant. The initial state is taken to be one isolated wavelength of a linear oscillatory mode extending from the centre (x=0) of one island to the adjacent X-point (x_{max}) and from the tearing surface (y=0) to a large distance (y_{max}) such that the perturbation is negligible and is decaying exponentially with y. Symmetry boundary conditions are applied at x = 0, x = x_{max}, y = 0, and a non-uniform grid is used in the y-direction with a concentration of grid-points near y = 0 in order to resolve the resistive layer.

Figure 1.2.5 plots the reduction $\Delta E_m = E_{mo} - E_m(t)$ in the magnetic energy $E_m(t)$ stored in the shear layer, where $E_{mo} = E_m(O)$. Except for the constant ψ solution, the energy that has been released by the end of the computation is between 8% and 27%. It can also be seen that the longer the wavelength ($\lambda = 2\pi a/\alpha$), the more magnetic energy is ultimately converted, even though the conversion rate is slower at first.

Figure 1.2.6 shows the formation near the X-point of a secondary flow vortex in the opposite sense to the initial linear vortex. When S and the wavelength are large enough the secondary flow can create a second magnetic island near the original X-point. Also, one finds intense current filaments and electric fields near the X-points. At the same time for long wavelengths (α = ka = 0.05) the width of the magnetic island grows to more than twice the initial shear layer width (a) by the end of the computation, even though nonlinear saturation has not yet occurred.

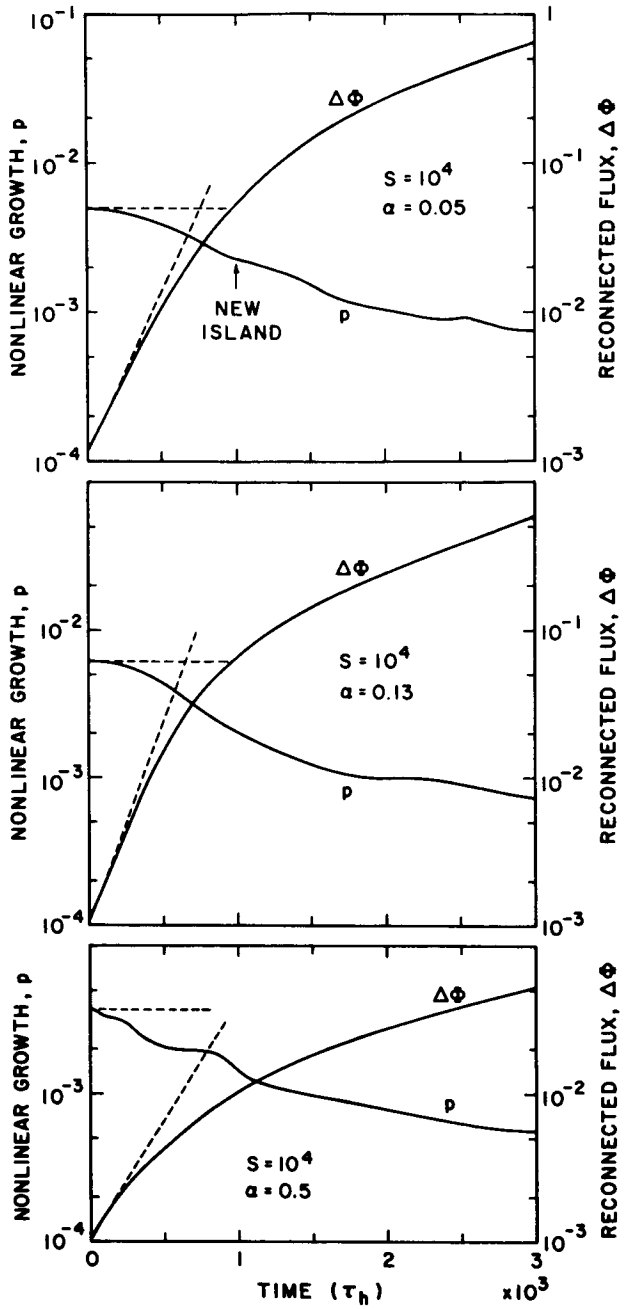

Figure 1.2.5 a) Nonlinear growth rate (p) and reconnected flux ($\Delta\phi$) as functions of time in units of the Alfven time ($\tau_h = a/V_A$) for the tearing instability of one island at a Lundquist number (s) of 10^4 and several values of the dimensionless wavenumber (α = ka).

1.2.4 Emerging Flux and Moving Satellite Sunspots

1.2.4.1 Their Two Roles

Small regions of emerging flux and small satellite sunspots are often observed before flares. They signify the interaction of separate magnetic flux systems, in the first case by means of a vertical motion and in the second case via a horizontal motion, but in either case the effect is similar, namely the pressing of one flux system against another and the creation of a current sheet at the interface at some height h.

The first role of such flux evolution is to *create small flares* when the current sheet reaches a critical height such

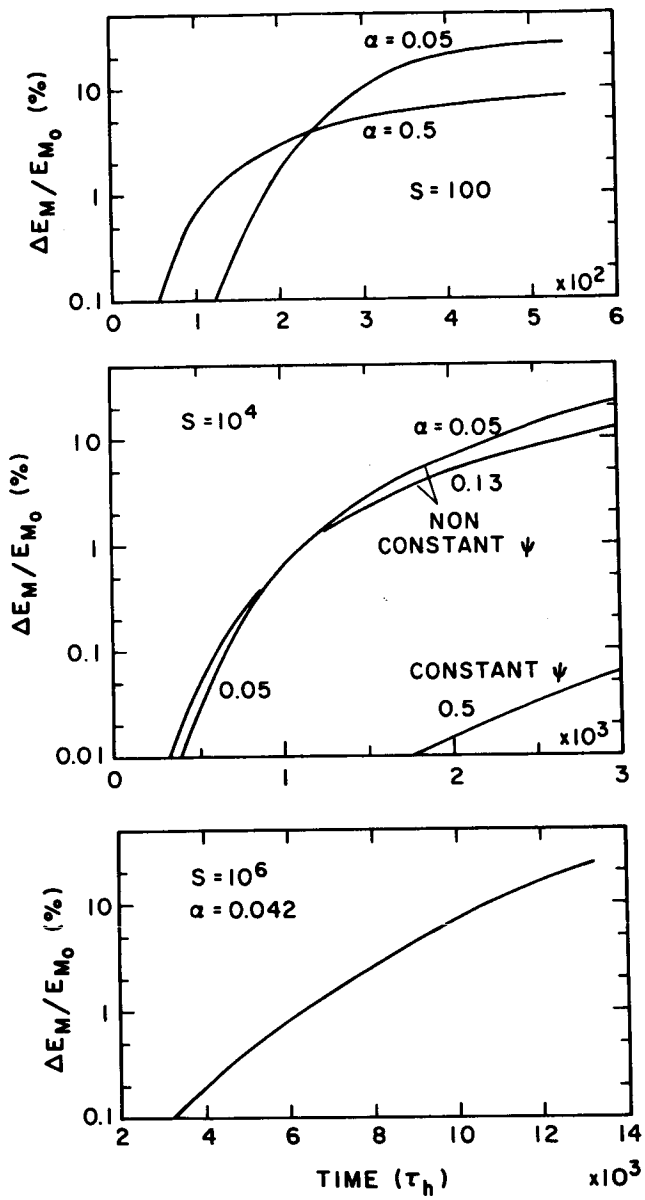

Figure 1.2.5 b) Temporal behavior of the percentage of magnetic energy removed from the shear layers (from Steinolfson and van Hoven 1984).

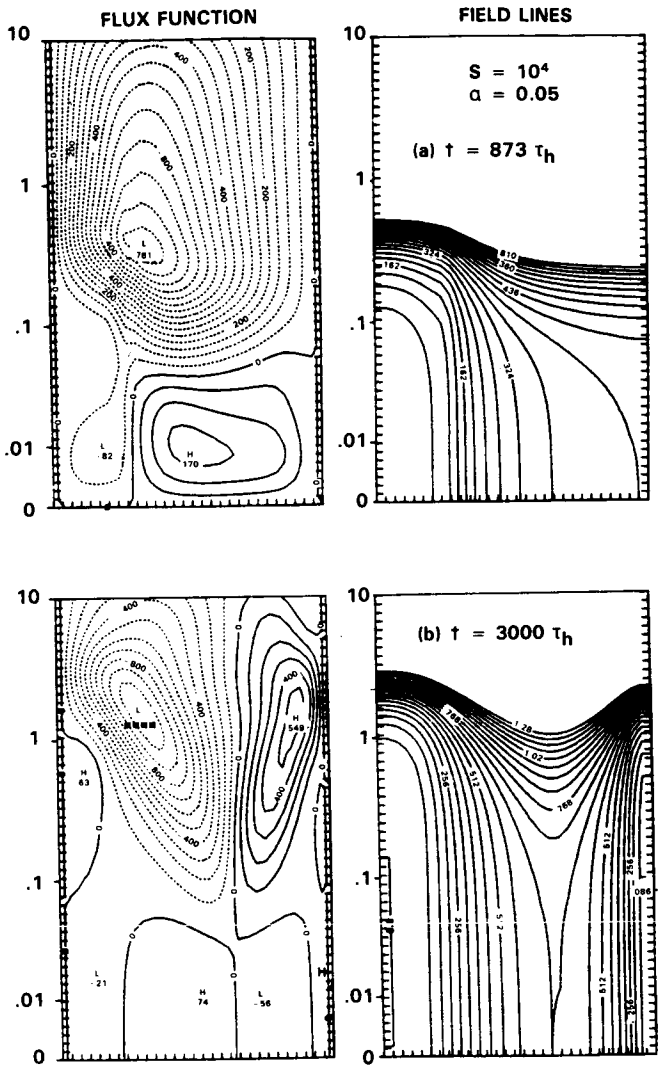

Figure 1.2.6 Stream function (left) and magnetic field lines (right) at two times during nonlinear tearing, illustrating the formation of a new magnetic island. Dashed curves represent a clockwise flow (the modified linear vortex) and solid curves an anticlockwise flow (the new vortex).

that the current density exceeds the threshold for the onset of microturbulence. This has been estimated by solving the energy balance equation within the sheet and so deducing the resistivity from the temperature (Heyvaerts, Priest and Rust 1977, Milne and Priest 1981).

The second role of emerging flux and moving satellites is thought of as a trigger of large flares by initiating energy release in a much more extensive overlying field. In particular, emerging flux may push up against a magnetic arcade containing an active-region filament until it goes magnetically unstable of its own accord (§1.2.6). Alternatively, it may tear away some of the overlying field lines that are helping to stabilise the arcade, or it may cause a large-scale reconnection by creating a small region of enhanced resistivity.

1.2.4.2 Numerical Experiment

Forbes (Forbes and Priest, 1984 submitted) has recently conducted the first numerical experiment of emerging magnetic flux by solving the resistive MHD equations with a code that is especially designed to treat shock waves well. The initial state consists of a uniform horizontal magnetic field

in a numerical box with free-floating conditions on the top and sides. New oppositely directed flux is forced in through the base rather rapidly at a speed of $v_A/8$, and the magnetic Reynolds number is 2000. The resulting magnetic and flow patterns are shown in Figure 1.2.7. In the first three panels the flux emerges and reconnects, with internal energy being converted to the kinetic energy of fast jets of plasma. At t=4 the emergence of new flux through the base is halted, but the flux continues to rise and enters a highly dynamic stage as it loses quasi-equilibrium. The magnetic field lines pinch off near the base and form a plasmoid, which ultimately disappears as the field reduces to a potential state.

Figure 1.2.8a presents a time-development of the mass density contours, showing the dense emerging flux region and, especially at t = 3.29, the two regions compressed by the shock pairs extending from the central current sheet. This sheet is longer than expected for steady Petschek-Sonnerup reconnection, indicating that reconnection is taking place at this time in a *flux pile-up regime* (§1.2.3.1). The top panel of Figure 1.2.8b gives the heights of the neutral lines as functions of time, with continuous and dashed curves referring to X- and O-points, respectively. It can be seen that at t=4 a pair of such points is created and at t=14 a pair is annihilated. The lower panel indicates the electric field as a function of time at the X-points. Just before t=4 it shows the onset of an *impulsive bursty regime* (§1.2.3.1), with the electric field having impulsive spikes in excess of the steady Petschek value.

Since the electric field at the X-line is a direct measure of the reconnection rate (i.e. the rate at which closed flux in the emerging region is converted into open flux), the variation of E_0 in Figure 1.2.8b gives an indication of the rate at which magnetic energy is converted into kinetic and thermal energy. During the *impulsive bursty regime* from t =

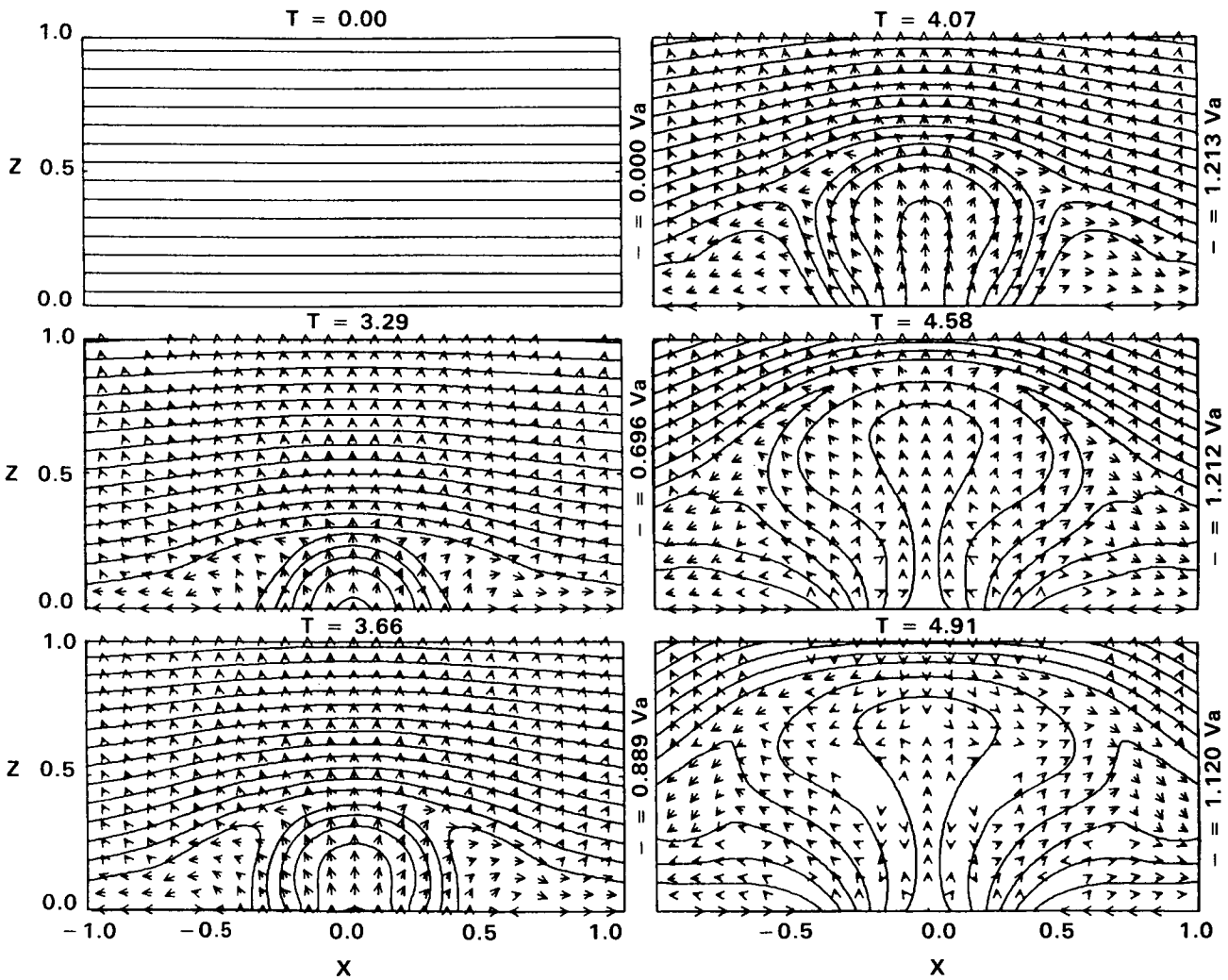

Figure 1.2.7 Magnetic field lines and plasma flow vectors for an emerging flux numerical experiment. At the top of each panel the time is indicated in units of the Alfven travel time across unit distance, and at the right the maximum flow speed is given. (From Forbes and Priest, 1984).

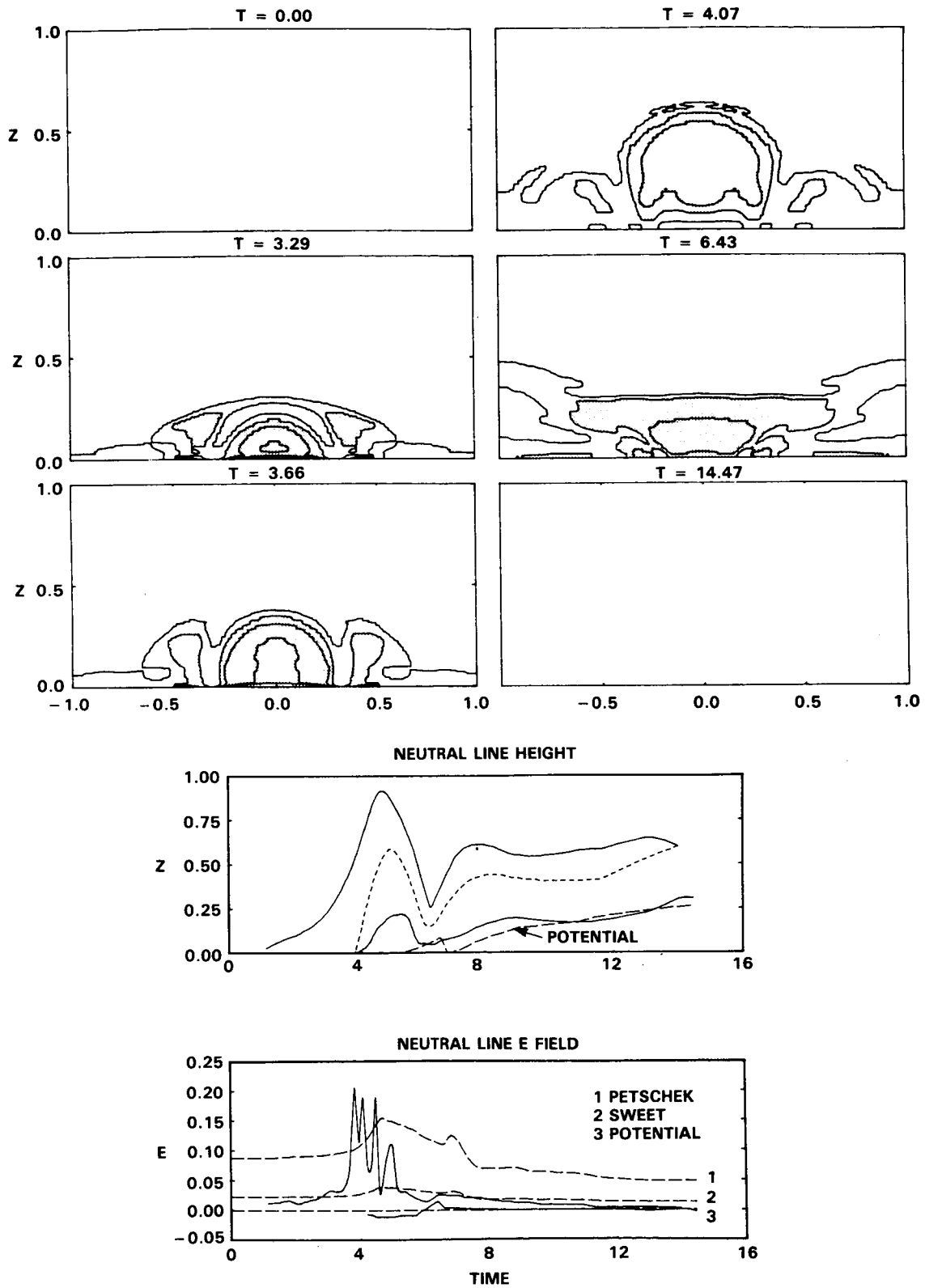

Figure 1.2.8 (a) Mass density contours. (b) Height and electric field of the neutral lines. (From Forbes and Priest, 1984).

3.7 to 4.5 there is a rapid release of magnetic energy over a period of about an Alfven scale-time, while before and after this period there is a slower release on the order of the tearing-mode time-scale. That this sequence is suggestive of the flare cycle of pre-flare, impulsive, and main phases is possibly not a coincidence. Instead it seems more likely that structures which incorporate both ideal MHD and resistive instabilities (or, alternatively, non-equilibrium states) will show fluctuations in the reconnection rate on both Alfven and tearing-mode time scales.

1.2.4.3 Current-Driven Instabilities

At the workshop, J. Karpen presented an investigation of the potential role of current-driven instabilities in producing brightenings and general preheating of the plasma in the preflare coronal loops (Karpen and Boris, 1985, submitted). This analytical work calculates the temporal evolution of the ambient plasma characteristics in an emerging, expanding flux tube with an axial magnetic field and electric current. In lieu of focussing on a specific current-driven instability (CDI), they constructed a "generic" CDI with a typical on/off cycle and associated heating. The magnetic-field configuration of an emerging flux tube is simulated by moving two point sources of magnetic flux away from a common origin with constant velocity. The density evolution is derived by considering the mass influx required, but not necessarily attained, for equilibrium in the expanding loop; thus, a range of mass flow rates into the tube is allowed, the zero mass flow yielding complete mass conservation. The temperature evolution is determined by the energy equation, which includes the effects of volumetric heating, intermittent heating due to the CDI, radiation, thermal conduction, and adiabatic cooling. The threshold criterion for the onset of the CDI heating depends solely on the characteristics of the beam current and ambient plasma, and operates under the assumption of marginal stability (e.g., Manheimer and Boris, 1977). Calculations were performed with fast and slow footpoint-separation rates, and with high, intermediate, and low mass-flow rates. The results show a variety of temperature behaviors: in particular, some cases include a single episode of excess CDI heating, lasting for tens of seconds, while others manifest temperature oscillations throughout a large fraction of the simulation period. These types of activity are reminiscent of the patterns of preflare brightenings often observed in the EUV, soft X-ray, and microwave regimes before flare onset (§1.3). The authors plan to use the NRL Dynamic Flux Tube Model (cf. Mariska *et al.*, 1982) to obtain more detailed calculations of the effects of the CDI on the dynamics and energetics in the expanding loop.

1.2.5 Main Phase Reconnection in Two-ribbon Flares

The overall magnetic behaviour during a large two-ribbon event is believed to be as follows. Throughout the *preflare phase* a large flux tube (containing an active-region filament) and its overlying magnetic arcade rise slowly. The rise may be caused by an ideal eruptive instability when the twist in the flux tube or its height become too great (Hood and Priest, 1980, Hood 1984a). Alternatively, it may be due to magnetic nonequilibrium when the equilibrium of a curved tube ceases to exist (Parker 1979, Browning and Priest 1975, §1.2.6.1) or it may be triggered by emerging flux.

The *onset* of the flare itself coincides with the start of the much more rapid eruption of the filament. It probably occurs because the magnetic field lines of the stretched out arcade start to reconnect below the filament (Priest 1981a, 1981b). The linear tearing of the field lines leads on to the fast Petschek and impulsive bursty regimes of reconnection, as described below (Figure 1.2.9). During the *main phase*

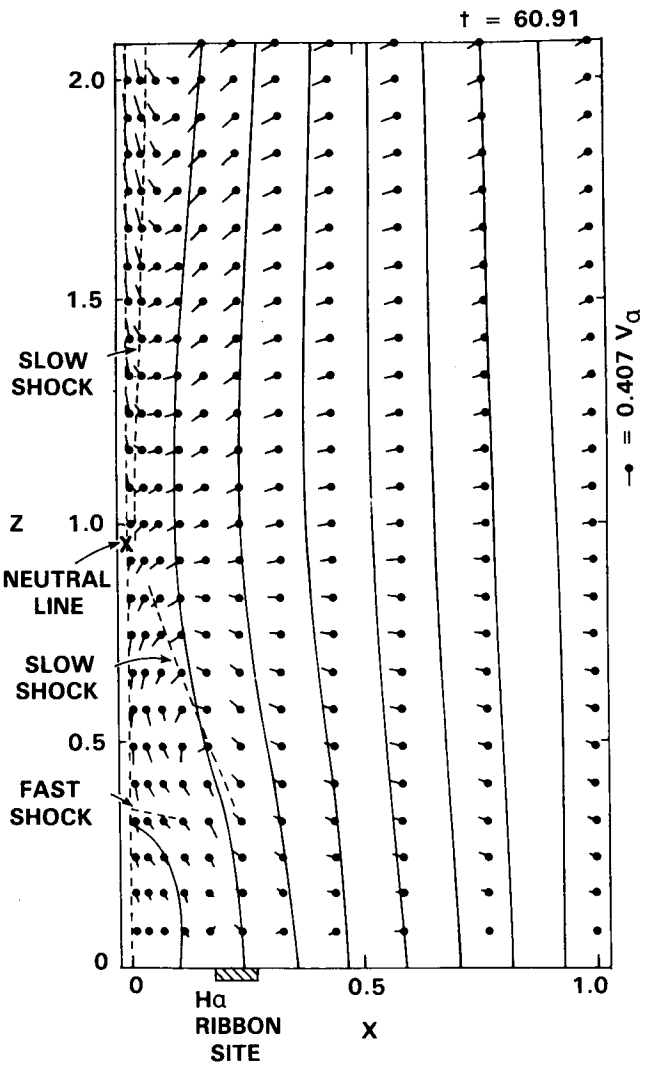

Figure 1.2.9 Magnetic field lines and flow velocity vectors at a quarter of the grid points during the Petschek phase of quasi-steady line-tied reconnection. (Forbes and Priest, 1984).

the reconnection is thought to continue and create hot 'post'-flare loops with Hα ribbons at their footpoints as the field closes down. The source of the immense mass of plasma that is subsequently seen to be falling down along cool 'post'-flare loops below the hot loops is an upflow of plasma from the chromosphere along the open field lines before they reconnect (Kopp and Pneuman 1976). The cause of the upflow may well be evaporation driven by thermal conduction or by fast particles that are accelerated at the shocks associated with the reconnection process. Furthermore, it has now been shown that these slow magnetoacoustic shocks can heat the upflowing plasma to the temperatures observed in the hot loops of up to twenty million degrees (Cargill and Priest 1982).

A numerical experiment on the line-tied reconnection that takes place below the erupting filament has been undertaken by Forbes (1982, 1983a, 1983b). He starts with open, stretched out and oppositely directed magnetic field lines in equilibrium and solves the 2D resistive MHD equations for the subsequent development of the right-hand half of the structure. The base of the numerical box is line-tied. Its left-hand edge is an axis of symmetry, and free-floating conditions are imposed on the other two sides.

First of all, the sheet tears near the base and the magnetic field lines start to close down with the X-type neutral point rising and a plasmoid being ejected from the top of the box. In the nonlinear development, reconnection enters a quasi-steady Petschek regime, which is shown in detail in Figure 1.2.9. The decrease of magnetic field strength and convergence of the flow vectors as the reconnection point is approached are characteristic of a fast-mode expansion associated with a Petschek-type of regime (§1.2.1.2). Also, the fast shock in the downflowing jet may be important for particle acceleration. In the subsequent development the sheet thins and the Petschek mode goes unstable, with the reconnection entering an impulsive bursty regime. Secondary tearing creates a new pair of O and X points, and reconnection at the upper X dominates so that the O is moved down and coalesces with the lower X. Meanwhile, a new pair appears and the process of creation and annihilation of neutral point pairs is repeated. The energy release in this process is faster than the steady Petschek rate, and it occurs in the impulsive manner that is observed in many flares.

1.2.6 Magnetic Instability Responsible for Filament Eruption in Two-Ribbon Flares

1.2.6.1 Loop Configuration

Many people have modelled the preflare magnetic configuration by a single loop and have investigated its stability, with applications to both small simple-loop flares and large two-ribbon flares in mind. Many such stability analyses have been undertaken neglecting for simplicity the curvature of the loop and regarding it as a straight cylinder (e.g., Raadu 1972, Hood and Priest 1979, Einaudi and Van Hoven 1981). Line tying of the ends of the loop in the dense photosphere is an important stabilising effect which makes the perturbation (ξ) vanish there. It keeps the loop stable until the amount of twist in the loop exceeds a critical value, typically 2π or more, depending on the particular equilibrium. The most complete analyses of this type have so far been carried out by Hood and Priest (1981) and Einaudi and Van Hoven (1983). The perturbed equation of motion is solved numerically to give the threshold twist for instability.

The effect of curvature on the equilibrium of an isolated slender coronal loop has also been considered in a simple model (Parker 1979, Browning and Priest 1985) which balances tension and buoyancy. One finds that the variation of the height H of the loop summit with the footpoint separation W is given by

$$\tan^2 \frac{W}{2\Lambda} = e^{H/\Lambda} - 1, \qquad (1.2.4)$$

where Λ is the gravitational scale height. Thus, as the footpoints move apart (W increases) the summit rises (H increases) until, as W approaches $\pi\Lambda$, the loop summit floats up indefinitely. For large footpoint separations there is no equilibrium at all. Including an external magnetic field lowers the buoyancy force and therefore the summit height, but it doesn't change the critical footpoint separation. Including a twist in the loop lowers the magnetic tension and so increases the summit height. It also lowers the critical width and changes its nature to a nonequilibrium point.

1.2.6.2 Arcade Configuration

For two-ribbon flares the preflare magnetic configuration has been modelled more accurately by a coronal arcade. In particular, the effect of line tying has been included in models of force-free arcades (Migliuolo and Cargill 1983, Hood and Priest 1980, Birn and Schindler 1981, Ray and Van Hoven 1982, Hood 1983a, Cargill *et al.*, 1984). The original analysis (Hood and Priest 1981) considered various classes of ideal perturbations and found that a simple arcade with its magnetic axis below the photosphere is always stable to those classes. It also appears to be stable to resistive modes usually (Hood 1984, Migliuolo and Cargill 1983). However, arcades with their magnetic axis a distance d above the photosphere are more interesting, since they are more likely to represent configurations within which an active-region (or plage) filament can form (Hood and Priest 1979). Such filaments are quite different from the large quiescent filaments and form along flux tubes. They are indicators of a highly sheared field and very often erupt before two-ribbon flares, slowly at first and then much more rapidly at flare onset. This type of coronal arcade (whose cross-section contains a magnetic island) is found to become unstable when either the height of the magnetic axis (and therefore of the filament),

or the amount of twist become too great (Hood and Priest 1981). This suggests that the eruption of the arcade may be caused by a *spontaneous eruptive instability when the filament height or the magnetic shear become too great.*

Recently, attention has been focussed on magnetohydrostatic arcades with a force balance between the Lorentz force, a pressure gradient and gravity. For a two-dimensional isothermal arcade in which the variables are independent of the direction z along the arcade, the magnetic field components can be found, especially in the limit as H approaches infinity such that the gravitational force is negligible (Low 1979, Heyvaerts *et al.*, 1982, Priest and Milne 1980, Zweibel and Hundhausen 1982, Melville *et al.*, 1983, 1984).

Having obtained the equilibria for magnetostatic arcades, it is important to analyse their stability, since an arcade must be stable if it is to store magnetic energy prior to flares. On the other hand, it is also necessary that this energy can be released by an instability when some critical threshold is reached. The stability of arcades can be studied either by the energy method or by solving the equations of motion. Using the energy method Schindler *et al.* (1983) and Hood (1984a, 1984b) independently obtained a sufficient condition for stability. For free-flow boundary conditions (see below) this condition also becomes necessary when there is no axial field ($B_z = 0$).

The strong stabilising influence of the dense photosphere, known as line-tying, has been modelled in two different ways, either by setting the perturbation ($\xi_\perp$) perpendicular to the magnetic field at the photospheric footpoints equal to zero or by making the total perturbation ($\xi_\perp + \xi_\parallel$) vanish there. The physical argument is that the high density (and low temperature) does not allow the photosphere to move in response to disturbances that propagate from the corona. For example, assuming the ratio of photospheric to coronal wave speed to be 10^3, 99.6% of the energy of a non-resonant MHD wave propagating from the corona should be reflected back and only 0.4% transmitted. It is generally agreed that line tying makes perturbations that are perpendicular to the magnetic field vanish at the photosphere for perfect reflection. However, the condition on perturbations parallel to the magnetic field is more controversial (Cargill *et al.*, 1985 submitted). The two main choices are to regard the ends as being rigid and set $\xi = 0$ (e.g., Hood and Priest 1979) or to allow free flow through the ends ($\nabla \cdot \{\xi e^{-y/H}\} = 0$ for an isothermal plasma). Many results in the literature differ because of the choice of this parallel boundary condition as well as the choice of equilibrium.

By solving the equations of motion with free-flow boundary conditions parallel to the magnetic field Migliuolo *et al.* (1984), have demonstrated that arcades with $B_z = 0$ are unstable to interchange modes with very short wavelength (λ_z) along the arcade. This instability may be important for the small-scale structure of the corona rather than for global flare instability. They also showed that, if B_z is non-zero, the arcade becomes unstable when the pressure gradient is large enough, a result which may account for the second stage of a double impulsive flare, in which the second part of the flare occurs after plasma has been evaporated up to the corona by the first part.

More recently, the work has been extended to compare the stability thresholds that result from free-flow and rigid end conditions (Cargill *et al.*, 1985, submitted). For cylindrically symmetric equilibria the presence of a rigid boundary gives rise to substantial differences in the stability thresholds. Equilibria with $B_z = 0$ may be either stable or unstable, depending upon the exact details of the equilibrium and the ratio of the specific heats (γ). Inclusion of shear (B_z) is stabilising, and for the equilibria considered a small amount of shear is sufficient to stabilise all the equilibria. Physically, the rigid conditions do not permit incompressible modes, and so there is an increase in the potential energy due to compression of the plasma. Clearly, the difference in the results from two sets of boundary conditions makes it important to understand the real nature of line tying, and to model it adequately (Cargill *et al.*, 1985, submitted).

Hood (1983b) has considered the arcade equilibrium

$$A = A_0 \cos\left(\frac{x}{4H}\frac{\sin Y}{Y^{1/2}}\right) \qquad (1.2.5)$$

where

$$Y = 2\beta H \exp(-1/2\ y/H) \qquad (1.2.6)$$

and $(2\beta H)^2$ is the plasma beta. This is a special case of the class considered by Zweibel and Hundhausen (1982), and the field lines are shown in Figure 1.2.10a. As the base pressure (and therefore β) increases, so the magnetic field lines bow outwards, and eventually for $2\beta H > 1.15$ a magnetic island appears (Figure 1.2.10b). When the pressure is so large that $2\beta H > \pi$ the upper field lines become detached from the photosphere and the configuration ceases to be physically realistic. When the magnetic island is present, Zweibel (1981) has shown that such fields tend to be unstable. Hood (1983b) has extended her analysis to include the effect of magnetic tension, which makes the field stable for small β.

It should be stressed that stability analyses of the above type may be used to estimate the amount of magnetic energy that may be stored in the corona in the stable state. The equilibria that are considered are certainly not accurate representations of active-region fields (see §1.3), but they do typify their expected properties.

1.2.6.3 Prominence Models

Recently, Malherbe (Malherbe and Priest 1983, Malherbe *et al.*, 1983) set up some new current sheet models for quiescent prominences using complex variable theory. Figure 1.2.11a,b shows two models of the Kippenhahn-Schluter type, while Figures 1.2.11c,d indicate some of the Kuperus-

4. The stability analyses imply that an arcade can become unstable when either its height or twist or plasma pressure become too great.

1.3 PREFLARE MAGNETIC AND VELOCITY FIELDS

M.J. Hagyard, V. Gaizauskas, G.A. Chapman, A.C. deLoach, G.A. Gary, H.P. Jones, J.T. Karpen, M.-J. Martres, J.G. Porter, B. Schmieder, J.B. Smith, Jr., and J. Toomre

A description of the structure, dynamics and energetics of the preflare state depends on our ability to characterize the magnetic and velocity fields of the preflare active region. In this SMM Workshop, we fortunately had at our disposal many sets of coordinated SMM and ground-based observations of magnetic and velocity fields from the photosphere, chromosphere, transition region and corona to aid in this characterization. At the outset we decided that several aspects of these fields are of special interest to the preflare state: configurations in the magnetic and velocity fields that seem peculiar to flaring active regions; the existence of shears (in both the magnetic and velocity fields); the occurrence of emerging flux. Some questions naturally arise concerning these topics. Do flares occur in active regions where the magnetic field is force-free (currents are field-aligned), non-force-free or both? If it is force-free, can it be specified by a constant-alpha? [Alpha is the ratio between current density and field strength]. Is magnetic shear correlated with the occurrence of flares and, if so, is there a critical value of this shear? What is the role of the resulting electric currents? What are the preflare characteristics of the velocity field and how do they evolve? What is the spatial and physical correlation between sheared velocity and magnetic fields? What are the conditions necessary for emerging flux to trigger a flare? What growth rates of flux are significant? How does the flux emerge into the corona?

Although we did not find answers to all these questions, we made significant progress in many areas. We found that the preflare active region is very dynamic, exhibiting recurrent mass surges and intermittent heating events at many sites. In one case, that of an active region not particularly productive of large flares, the structure of the magnetic field was best represented by a nonlinear force-free field; for a particularly flare-productive region, there were indications that, subject to certain restrictions on the boundary conditions, the field was non-force-free, exhibiting a measurable Lorentz force. We also found that both the magnetic and velocity fields are sheared in flaring regions; the shear of the magnetic field attained maximum values at the sites of flare onset, whereas the velocity field sometimes exhibited an unusual vortical structure at these sites. These sheared magnetic fields produced persistent, large-scale concentrations of electric currents at the flare sites; numerical values for the magnitudes of these currents provided input to models describing preflare brightenings based on joule heating or current-driven instabilities. Finally, we found the role of emerging flux in flares to be ambivalent, providing an obvious triggering of some classes of flare while having no role in the flare process in others.

In describing these various results the material has been arranged as follows. We begin with a characterization of the preflare magnetic field, using theoretical models of force-free fields together with observed field structure to determine the general morphology. We then present direct observational evidence for sheared magnetic fields. The role of this magnetic shear in the flare process is considered within the context of an MHD model that describes the buildup of magnetic energy, and the concept of a critical value of shear is explored. The related subject of electric currents in the preflare state is discussed next, with emphasis on new insights provided by direct calculations of the vertical electric current density from vector magnetograph data and on the role of these currents in producing preflare brightenings. Next we discuss results from our investigations concerning velocity fields in flaring active regions, describing observations and analyses of preflare ejecta, sheared velocities, and vortical motions near flaring sites. This is followed by a critical review of prevalent concepts concerning the association of flux emergence with flares.

1.3.1 General Morphology of the Preflare Magnetic Field

It is generally accepted that magnetic fields are the ultimate source of the energy released in a flare (e.g., Svestka, 1976) and that this energy is stored in an active region prior to the flare as a result of the stressing of these fields into non-potential configurations We have accumulated observational evidence for such stressed fields, both on large and small scales, and studied the stressing processes which result in the eruption of a flare. We first discuss our studies of the general morphology of the preflare magnetic field.

A. Gary endeavored to classify the non-potential character of magnetic fields in active regions assuming that the fields are force-free, i.e., that the following relation is valid:

$$\nabla \times \underset{\sim}{B} = \mu_0 \underset{\sim}{J} = \alpha \underset{\sim}{B}. \qquad (1.3.1)$$

Several active regions observed during SMM were modeled using the force-free formulation developed by Nakagawa and Raadu (1972), who assumed that the parameter α is spatially invariant. One of these regions, AR2684, was of particular interest since it was observed by instruments on a Lockheed rocket flight at 20:30 UT on September 23, 1980, as well as by SMM and ground-based instruments. Although the flare activity in the region was relatively minor, several C- and M-class flares occurred on the 23rd and 24th, the largest being a 1B/M1 event at 07:28 UT on the 24th.